



**Environmental
Science
Nano**

**Insight into the Pressure-induced Displacement Mechanism
for Selecting Efficient Nanofluids in Various Capillaries**

Journal:	<i>Environmental Science: Nano</i>
Manuscript ID	EN-ART-05-2020-000462.R1
Article Type:	Paper

**SCHOLARONE™
Manuscripts**

Insight into the Pressure-induced Displacement Mechanism for Selecting Efficient Nanofluids in Various Capillaries

Xiao Wang ¹, Zhiliang Zhang ¹, Jun Zhang ² and Jianying He ^{1,*}

¹ NTNU Nanomechanical Lab, Department of Structural Engineering, Faculty of Engineering, Norwegian University of Science and Technology (NTNU), 7491 Trondheim, Norway

² School of Materials Science and Engineering, China University of Petroleum, Qingdao, Shandong, 266580 China

Corresponding author:

Jianying He

Email: jianying.he@ntnu.no

Tel.: +47-93804711

Abstract

Designing fluids to regulate two-phase displacement has been of great interest because of its roles in groundwater remediation, oil recovery and water desalination. Currently, the displacement efficiency of fluids is observed to depend on the surface properties of capillary and external pressure. Herein, the pressure-induced displacement mechanisms in various capillaries are investigated by molecular dynamics simulations. Our results suggest that the surface wettability and pressure are crucial to the displacement performance of fluids. Specifically, reducing the interfacial tension of fluids is beneficial to displacement efficiency in hydrophobic capillary, while increasing viscosity of fluids favors for hydrophilic capillary. Based on our proposed mechanisms and considering the capillaries wettability, three types of nanofluids are designed to improve the displacement efficiency for different capillaries. Our results are significant for understanding fluids flow phenomenon and provide an efficient way to design the target fluids for numerous applications.

Keywords: Two-phase displacement; Pumping pressure; Nanoparticles; Wettability; Resource Recovery; Molecular dynamics simulation.

1. Introduction

Multiphase flow in capillary is a common and fundamental process in both nature and industrial fields,¹ such as groundwater remediation, sea water desalination,² ink jet printing, and nanofluidics.³⁻⁵ For fluids flow in these processes, external pressure is often applied to improve flow velocity and displacement efficiency.⁶ Taken the oil field as an example, increasing the pumping pressure of injecting fluid can improve the oil recovery efficiency from the reservoirs. However, as flooding pressure reaches a specific high value, considerable amount of oil would be trapped in the reservoir due to “fingering” phenomenon of the injecting fluid. Overcoming the “fingering” to increase the production of the residual oil is a hot topic in the research of petroleum engineering.

To date, much research efforts have been devoted to optimizing the two-phase displacement process, such as refining the external forces,⁷⁻⁹ changing the composition of capillary surface,¹⁰⁻¹² and adjusting the properties of fluids¹³ like viscosity and interfacial tension. Among others, adding extra chemicals (surfactant, polymer) can effectively adjust the property of injecting fluids, and meanwhile change the composition of capillary surface with their adsorption, which is thus efficient in regulating two-phase displacement process.^{14, 15} Currently, the development of new chemical fluids to regulate two-phase displacement involves a major challenge, as many studies observed that the efficiency of chemical fluid is capillary dependent. For example, according to the worldwide enhanced oil recovery (EOR) survey, not all the reservoirs can adopt same chemical fluids, and the performance of a specific chemical fluid varies significantly in different capillaries.¹⁶ Therefore, selecting and designing injecting fluids targeted to the specific capillary is necessary in two-phase displacement applications.

Despite the clear experimental evidences,^{17, 18} the capillary-dependent efficiency of various chemical fluids is not well understood at atomic level, as the experiment studies by core flooding is not a straightforward process.^{19, 20} Computation simulation, especially atomistic and molecular modeling, enables visualization of the displacement process and can provide the atomistic details of fluid flow in confined channel.²¹⁻²⁶ Wu et.al²⁷ investigated the flow of water confined in nanopores with different wettability and dimensions by molecular dynamic (MD) simulations. An accurate model was proposed to calculate fluid flux and compared the results with theoretical analysis. Towards this end, we adopt all-atom simulation to investigate the displacement mechanism for fluids in different capillaries. And more importantly, according to our newly proposed mechanism, three types of nanofluids (a class of

1
2
3 fluids engineered by dispersing nanoparticles (NPs), which becomes emerging interests
4 recently and are reported to have a great potential to modify the dynamic displacement process
5 (22, 28-30) are specifically designed to match the properties of capillary surface and improve their
6 displacement efficiency.
7
8
9

10 Initially, the threshold capillary pressure needed for water entering into oil-filled capillary
11 is calculated, and the relationship between the threshold capillary pressure and wetting
12 properties of capillary is established. Then, the forced two-phase flow behavior in capillary
13 ranging from hydrophobic to hydrophilic is analyzed to reveal the involved displacement
14 mechanism. Accordingly, the capillary-dependent efficiency of three type NPs is discussed.
15 Our findings provide physical insights into the flow behavior in capillary and design guidelines
16 for targeted applications.
17
18
19
20
21
22

23 **2. Model and Simulation Details**

24 **2.1 Model systems**

25 All-atom simulation system consisting of piston, displacing phase (water), displaced oil
26 phase (decane), and solid capillary was built to study the forced two-phase displacement in the
27 capillary, as shown in Figure 1. A single cylindrical capillary with radius $R = 25 \text{ \AA}$ was
28 constructed by removing all atoms along the y-axis center of a silicon block in dimensions of
29 $L_x = L_z = 65.1684 \text{ \AA}$ and $L_y = 194.1475 \text{ \AA}$, and the atomistic parameters were not fixed during
30 simulation. The displaced phase in cylindrical shape with 20 \AA in radius, including 920 decane
31 molecules, was placed in the nanochannel to fill up the cylindrical capillary.³¹ The atomistic
32 parameters from CHARMM force field were used for oil molecules.^{32, 33} Equilibrium MD
33 simulations were carried out to obtain steady-state distribution of oil in capillary. Displacing
34 phase was composed of 20,000 water molecules. The simple point charge/extend SPC/E model
35 was adopted for water molecules.³⁴ To mimic the external pumping pressure, a solid piston
36 layer constructed by copper block was placed at the left-hand side of the simulation box. There
37 were 650 atoms in the first layer of piston, and the cross-section area of block was kept the
38 same as the box. The periodic boundary conditions were used in MD simulations. Meanwhile,
39 a vacuum space served as buffer space for the displaced oil phase outside the capillary was
40 added to the right-hand side of the simulation box along y direction. This vacuum space was
41 large enough ($>250 \text{ \AA}$) to exclude the possible interaction between the displaced oil phase
42 outside the capillary and the piston as well as water phase.
43
44
45
46
47
48
49
50
51
52
53
54
55
56
57

58 **Figure 1**

59 **2.2 Computational Details**

Large-scale atomic/molecular massively parallel simulator (LAMMPS) package was employed to perform all the atomistic simulations.³⁵

The well-known standard pairwise 12-6 Lennard-Jones (L-J) potential was employed to describe the nonbonded intermolecular interactions, as stated in Equation (1). The long range coulombic interaction was described by Equation (2).

$$U_{LJ} = 4\epsilon_{ij} \left[\left(\frac{\sigma_{ij}}{r_{ij}} \right)^{12} - \left(\frac{\sigma_{ij}}{r_{ij}} \right)^6 \right] \quad (1)$$

$$U_{coulomb} = \frac{q_i q_j}{4\pi\epsilon_0 r_{ij}} \quad (2)$$

where ϵ_{ij} and σ_{ij} were the energy well depth and zero potential distance, r_{ij} represented the distance between atom i and j , q_i and q_j were charges on atom i and j , and ϵ_0 was vacuum permittivity. The interactions between oil-water, water-capillary and oil-capillary were calculated by the Lorentz-Berthelot mixing rule, with cutoff of 10.0 Å.

To investigate the influence of surface properties of capillary on the displacement, the capillaries were constructed as ideal surfaces, and the characteristic energy ϵ_{sw} (water-capillary) was tuned from 0.1 to 0.4 kcal/mol (in 0.05 increment) to form super-hydrophobic, hydrophobic and hydrophilic capillary.^{36,37} Here the wettability of capillary was defined based on three-phase contact angle (water-oil-capillary). The value above 150° meant super-hydrophobic capillary, and between 90° and 150° showed hydrophobic property, while below 90° was hydrophilic capillary. For the piston, the characteristic energy was set relatively small about 0.01 kcal/mol, indicating a weak interaction with water and a negligible effect on fluid transportation. A force along the y -axis was exerted on the piston to drive water molecules into the capillary and displace oil molecules out of the capillary. The pressure imposed on displacing fluid was calculated by dividing the total force by the cross-section area of piston. Atoms in the piston and the capillary were charge free. The vilification process about model was described in Supporting information.

All the systems were energy-minimized with steepest descent method, followed by simulations performed under NVT ensemble (constant number of particles, volume, and temperature). The temperature was controlled at 298 K by Nose-Hoover thermostat with 1.0 damping coefficient.³⁸ Newton's motion equation was integrated by velocity verlet algorithm. The long-range electrostatic interactions were compensated by using the particle-particle-particle-mesh (PPPM) algorithm with a convergence parameter of 10^{-4} .³⁹ Moreover, solid

1
2
3 capillary was kept rigid during the simulation to reduce simulation time. The simulation
4 configurations were visualized by VMD software.⁴⁰
5
6

7 **3. Results and Discussion**

8 **3.1 Threshold capillary pressure**

9
10
11 The threshold capillary pressure is crucial to quantify pressure needed for fluids
12 transporting into the capillary. To study the threshold pressure for different capillaries, water
13 molecules were pushed into the nanopore filled with oil molecules by applying a relatively
14 high pressure on the piston.⁴¹ According to our previous simulations,³⁶ the capillary with $\epsilon_{sw} =$
15 0.2 kcal/mol indicates hydrophobic property, and here is taken as an example to illustrate
16 calculation of threshold capillary pressure. Initially, water was injected into the capillary under
17 the pressure of 403.77 atm (the average force of 0.04 kcal/(mol·Å) on the piston). After 4.0 ns,
18 the front of injecting fluids reached distance 130 Å from the entrance of the capillary. Then,
19 the external force was removed and the piston was frozen for about 8 ns so that oil molecules
20 outside the capillary reached equilibrium (Figure 2 (a)). To quantify the equilibrium of system,
21 the amount of oil molecules outside the capillary is counted in Figure 2 (b). The number of
22 displaced oil molecules increases initially, and keeps in a nearly constant value after 3 ns,
23 indicating that the system has already reached equilibrium.
24
25
26
27
28
29
30
31
32
33

34 **Figure 2**

35
36 Here, the pressure at which displaced oil molecules starts to retract into the pore is
37 quantified as the threshold capillary pressure. Therefore, the average force exerting on the
38 piston decreases from 0.018 to 0.01 kcal/(mol·Å) to reduce pressure difference across fluids
39 interface in the capillary and obtain the threshold capillary pressure. Under each pressure, the
40 simulations were carried out at least 2.0 ns, and the dynamic number of oil molecules out of
41 the capillary is counted, as shown in Figure 3. When the average force is above 0.016
42 kcal/(mol·Å), oil molecules outside capillary has an apparent accumulation with time evolution.
43 As the average force decreases to 0.01 kcal/(mol·Å), the number of oil molecules outside the
44 capillary reduces with the increased time. In the case of the average force about 0.014
45 kcal/(mol·Å), the amount of oil molecules out of the capillary reach a dynamic equilibrium
46 state, indicating the relative force balance for fluids in capillary. Hence, the calculated
47 threshold capillary pressure is about 140.42 atm for $\epsilon_{sw} = 0.2$ kcal/mol capillary.
48
49
50
51
52
53
54
55

56 **Figure 3**

1
2
3 The same method is adopted to study the influence of wettability of the capillary on the
4 threshold pressure, and its relationship with the characteristic energy ε_{sw} is plotted in Figure
5 4(a) and the corresponding contact angle in Figure 4(b). It can be seen that the threshold
6 capillary pressure for water transporting into the capillary decreases with the increase of the
7 characteristic energy ε_{sw} . It suggests that higher pressure is needed for water flooding into
8 superhydrophobic and hydrophobic capillary (ε_{sw} smaller than 0.35 kcal/mol), while no
9 pressure is needed for hydrophilic capillary (ε_{sw} above 0.4 kcal/mol), where spontaneous
10 imbibition can occur. Meanwhile, when the characteristic energy is smaller than 0.2 kcal/mol,
11 i.e. superhydrophobic capillary, the threshold capillary pressure is relatively stable. While
12 above 0.2 kcal/mol, there is a linear relationship between the threshold capillary pressure and
13 the characteristic energy. Similar phenomenon is also observed in the relationship between
14 contact angle (methods to calculate contact angle is shown in Section S3 in supporting
15 information) and characteristic energy, as shown in Figure 4 (b), consistent with previous study.

42

Figure 4

3.2 Forced water-oil displacement mechanism

32 The pumping pressure and wettability of capillary have great influence on the forced
33 water-oil displacement in confined nanochannel, which is crucial to design the displacing
34 flooding for EOR process.⁴³ In order to reveal the underlying mechanism, the external
35 pumping force was increased from 0.08 to 0.24 kcal/(mol·Å) (in 0.04 increment) by controlling
36 the average force exerting on the piston. The wettability of capillary was tuned by increasing
37 characteristic energy ε_{sw} from 0.1 to 0.4 kcal/mol (in 0.05 increment), forming
38 superhydrophobic, hydrophobic and hydrophilic capillaries. Therefore, in total 35 systems
39 were adopted to study the forced water-oil displacement process.

Figure 5

47 The displacement process in three characteristic capillaries with different pumping
48 pressure is shown in Figure 5, and other simulation snapshots are shown in Section S5
49 (Supporting Information). In general, increasing pumping pressure promotes the water flooding
50 and facilitates the meniscus convexity or sharpness of the water front piercing into the oil phase
51 due to high velocity of injecting fluids. Compared with the phenomena in super-hydrophobic
52 capillary ($\varepsilon_{sw} = 0.10$ kcal/mol), water molecules in the hydrophobic capillary ($\varepsilon_{sw} = 0.25$
53 kcal/mol) move quickly into the oil phase with wavy flow. Regardless of pumping pressure,
54 there are always oil molecules stuck on the wall of super-hydrophobic or hydrophobic capillary

1
2
3 due to the weak interaction between water and capillary. For hydrophilic capillary ($\varepsilon_{sw} = 0.40$
4 kcal/mol), the formed meniscus is stable and moves slowly in the capillary at low pumping
5 pressure, which has potential to displace all the oil molecules near the wall and push the whole
6 oil cylinder moving along the capillary. However, under the relatively high pumping pressure,
7 the injecting fluid transports very fast through the oil phase and a considerable amount of oil
8 molecules remains in the capillary after water flooding.
9

10
11
12
13
14 The relationship between pumping pressure and content of extracted oil molecules from
15 the capillary is calculated and shown in Figure 5(c). Here, the position where same amount of
16 water molecules entering the capillary under different pumping pressure is treated as the
17 reference point, and the capillary with $\varepsilon_{sw} = 0.1$ kcal/mol is taken as an example. Thus, the
18 velocities of the piston moving from initial position to the final position depend on the choice
19 of fluids, and the end simulation time is distinct in various systems. There is an approximately
20 linear relationship between pumping pressure and number of oil molecules displaced from
21 capillary. This can be explained by Lucas-Washburn equation for two-phase displacement in
22 confined channel.⁴⁴ When the pumping pressure is higher, the total amount of extracted oil
23 molecules is much smaller despite more oil molecules at certain time and same amount of
24 injecting water molecules. Therefore, reducing the starting pressure is beneficial for EOR
25 process, which is also validated by other studies about CO₂ injection.⁶
26
27
28
29
30
31
32
33
34

35 From Figure 5 (b), the displacing fluid flow in hydrophobic and hydrophilic capillary at
36 high pumping pressure is unstable, and lots of oil molecules are left in the capillary. The
37 morphology of residual oil is crucial to design efficient fluids to improve displacement
38 efficiency. Therefore, the systems were equilibrated for sufficiently long time by fixing the
39 piston to display the distribution of residual oil. The obtained flow configurations after water
40 flooding are shown in Figure 6. In the hydrophobic capillary, the residual oil molecules tend to
41 connect and form a water in oil emulsion. Due to strong interaction between oil and capillary,
42 a thin oil layer is always sticking onto the capillary and difficult to be displaced by water
43 flooding. The critical point for hydrophobic capillary is to displace the adsorbed oil film on the
44 solid capillary. In contrast, the water molecules in the hydrophilic capillary would be adsorbed
45 onto the wall and displace oil molecules. After water flooding, the residual oil molecules
46 nucleate and grow up to large droplets, tending to form an oil in water emulsion, which is also
47 observed in experiments.^{17,45} Almost all the residual oil molecules in hydrophilic capillary can
48 be displaced if the time is long enough at low pumping pressure. The key point in hydrophilic
49 capillary is to improve displacement efficiency quickly at high pumping pressure.
50
51
52
53
54
55
56
57
58
59
60

Figure 6

According to the displacement process, two main displacement mechanisms are identified. In the hydrophobic capillary, the displacement process is dominated by the interaction between water and capillary, and the pivotal issue is to displace the oil film on the hydrophobic capillary. For the hydrophilic capillary, the water-oil displacement is dominated by fluids properties, such as interfacial tension and viscosity. Almost all oil molecules can be displaced at low pumping pressure, and then how to improve the oil displacement efficiency at high pumping pressure is important for hydrophilic capillary.

3.3 Selection of NPs for different wettability of capillary

Designing efficient fluids can increase the displacement efficiency in capillary, and the efficiency of fluids is dependent on the surface properties of capillary. According to the displacement mechanism discussed in section 3.2, the requirement for fluids properties is different for capillary with varied wettability. Here, three ideal types of NPs, hydrophilic, hydrophobic and Janus NPs, are examined as the candidates for the different types of capillaries to displace oil phase.⁴⁶⁻⁴⁹ The pumping pressure is fixed to 403.77 atm (exerting force = 0.04 kcal/(mol·Å)) for all the systems, and the details about constructing forced two-phase displacement system containing NPs are described in Section S6(Supporting Information).

Capillary number,²² a dimensionless parameter related with EOR process, can be adopted to select suitable NPs:

$$N_c = \frac{\eta_{inj} \times v}{\sigma_{ow}} \quad (3)$$

where η_{inj} is viscosity of displacing liquid (Pa·s), v is flow velocity (m/s), and σ_{ow} is interfacial tension between fluids. Increasing capillary number indicates the improved displacement efficiency of oil recovery.⁵⁰ Therefore, parameters in the equation can be tuned by adding NPs in hydrophobic and hydrophilic capillary to EOR.

Figure 7

For hydrophobic capillary, the key to enhance capillary number is to reduce the adsorption of oil layer onto the capillary, so that water can displace residual oil molecules. NPs can modify the capillary force, via tuning such as interfacial tension or three-phase contact angle. The effect of three types of NPs on the displacement process in hydrophobic capillary ($\varepsilon_{sw} = 0.25$ kcal/mol) is shown in Figure 7. From the flow behavior in Figure 7 (a), it can be seen that all the hydrophilic NPs are well dispersed in water phase. According to our previous simulations,⁵¹ dispersed hydrophilic NPs increase the viscosity of fluid phase, and thus enhance capillary

1
2
3 number of the fluids compared with base fluids. However, hydrophilic NPs, are difficult to be
4 adsorbed onto the capillary to overcome high pressure of the sticking oil thin layer.
5 Hydrophobic NPs are either dispersed in the water phase or transported into the oil phase but
6 not absorbed onto the capillary. NPs remained in the water phase tend to aggregate into bigger
7 ones and transport into the oil phase, while those transported NPs into the oil phase increase
8 the oil viscosity, resulting in the decreased displacement process.⁵¹ Therefore, hydrophobic
9 NPs are also difficult to alter the wettability of the capillary wall and to increase the exploration
10 of residual oil films. Once the Janus NPs are added into water flooding, some of them are
11 adsorbed onto the capillary wall, and while others stay at the front of the water-oil interface
12 during the displacement process. Taking a close observation of Janus NPs adsorbed onto the
13 hydrophobic capillary, the hydrophobic side orients into the capillary wall, while the
14 hydrophilic part of NPs directs to the water phase. The adsorption of Janus NPs pierces through
15 the oil layer sticking on the capillary wall, contributing to the wettability alteration of the
16 capillary, reducing the interfacial tension and thus enhanced oil recovery (Figure 7(b)).⁵² The
17 motion behavior of NPs in the capillary is closely related with the detailed displacement
18 mechanism for NPs, which has been discussed in our previous publications, and are
19 summarized in supporting information (Section S7). To compare the displacing efficiency of
20 water and nanofluids, the number of oil molecules displaced out of the capillary against with
21 simulation time are counted in Figure 7(c) for three types of nanofluids. When the piston moves
22 to the specific end positions (same end positions for all considered systems), the simulation
23 stops. Therefore, the simulation time is different for system with water and nanofluids. It is
24 clear that three kinds of nanofluids displace more oil molecules than water, demonstrating the
25 potential application of NPs in EOR process. Moreover, Janus NPs have better performance to
26 displace oil molecules in shorter time compared with other two counterparts owing to the
27 reduced capillary force.

46 **Figure 8**

48 In the hydrophilic capillary ($\varepsilon_{sw} = 0.4$ kcal/mol), low pumping pressure displaces all the oil
49 molecules out of the capillary, while high pumping pressure leaves lot of oil molecules in the
50 capillary after water flooding, as shown in Figure 5. The key point is to modify the fluids
51 properties to enhance the residual oil exploration, such as increasing the viscosity of water
52 phase at the same injection rate. According to our previous studies,^{51, 53} hydrophilic NPs have
53 a good performance than other types on the viscosity increase; therefore, only hydrophilic NPs
54 are studied to give an example. The effect of hydrophilic NPs on the water-oil displacement in
55
56
57
58
59
60

1
2
3 hydrophilic capillary is shown in Figure 8 (a) and (b). From Figure 8a, in pure water system,
4 the piston moves fast. At 1.8 ns, the piston has already reached the entrance of capillary with
5 all water molecules inside the capillary. However, in hydrophilic NPs system, due to the large
6 viscosity of this fluid, the piston moves relatively slow. At 1.8 ns, the piston is still away from
7 the entrance of the capillary. In 0 – 1.8 ns, for these two systems, though different amount of
8 displacing water molecules enter into the capillary due to the different velocity of piston, the
9 numbers of displaced oil molecules out of the capillary are always same at any simulation time
10 in this period (seen in Figure 8b). In other words, the oil exploration rate by hydrophilic NPs
11 flooding is comparable to that of pure water. Moreover, at 1.8 ns, in hydrophilic NPs system,
12 the piston still has some distance to move into the entrance of the capillary, which can push
13 more displacing water molecules into the capillary and result in more oil molecules displaced
14 out of capillary (1.8 to 2 ns in Figure 8b). Therefore, the hydrophilic NPs can displace more oil
15 molecules than water. This is attributed to that hydrophilic NPs increase the viscosity of water
16 phase, enhancing the sweeping efficiency of displacing fluids. These results indicate that
17 hydrophilic NPs have better performance to explore residual oil in the hydrophilic capillary.
18
19
20
21
22
23
24
25
26
27
28

29 The above analysis and discussion demonstrate that NPs can be adopted to enhance oil
30 recovery. Combining with the motion behavior of NPs in forced fluids flow, Janus NPs are
31 proposed for hydrophobic capillary, and hydrophilic NPs are suggested for hydrophilic
32 capillary. In this work, the ideal NPs are studied, and further investigation is needed to design
33 realistic NPs for EOR. For example, the specific types of NPs, the amount of NPs, the optimal
34 pumping pressures will all influence the NPs effect. Moreover, the simplified models are quite
35 different from real environment, and more factors like the component of oil, high temperature,
36 different salinity, should be considered in the future.
37
38
39
40
41
42
43

44 **4. Conclusion**

45 The forced displacement mechanism in hydrophobic and hydrophilic capillary is
46 investigated by all-atom molecular dynamics simulations. The effects of pumping pressure and
47 wettability of the capillary on the fluid flow process are explored initially to reveal the
48 displacement mechanism. It is found that the threshold capillary pressure for displacing fluids
49 into different wettability of capillary possesses linear relationship with characteristic energy
50 between water and capillary except for the super-hydrophobic ones. The pumping pressure
51 must be higher than threshold capillary pressure to enable the displacement process. However,
52 lowering the pumping pressure is beneficial to EOR. In hydrophobic capillary, the
53 displacement process is dominated by the interaction between capillary and water. An oil layer
54
55
56
57
58
59
60

1
2
3 is always stuck onto the capillary wall, and water flooding is piercing into oil phase with high
4 slip length at high pumping pressure, causing water in oil emulsions in confined channel after
5 flooding. The key point for hydrophobic capillary is to reduce interfacial tension or alter
6 wettability of solid capillary to improve displacement efficiency. In hydrophilic capillary, the
7 displacement of water-oil is dominated by fluids properties, such as interfacial tension and
8 viscosity. All the oil molecules are displaced from capillary at low pumping pressure due to
9 high interaction between water and capillary, while the increasing pumping pressure causes
10 residual oil molecules. The residual oil molecules coalesce to form oil in water emulsion after
11 water flowing. Designing fluids with higher viscosity is beneficial for displacement in
12 hydrophilic capillary.

13
14
15
16
17
18
19
20
21 Based on the displacement mechanism in different capillaries, three types of NPs,
22 hydrophobic, Janus and hydrophilic, are proposed to enhance displacement efficiency for
23 different capillaries. The results indicate that Janus NPs have better performance for
24 hydrophobic capillary, while hydrophilic NPs are favorable for hydrophilic capillary. The
25 researches not only uncover the forced fluids flow phenomenon, but also dawn on the basis for
26 designing efficient fluids for different types of reservoirs, which is significant for
27 understanding and designing suitable NPs or other chemicals for EOR process.

28
29
30
31
32
33
34 **Supplementary Materials:** The following are available online at <http://>.

35
36
37
38
39 **Acknowledgments:** This work is financially supported by the Research Council of Norway,
40 Aker BP ASA, Wintershall Norge AS via WINPA project (NANO2021 and PETROMAKSII
41 234626), and National Natural Science Foundation of China (U1663206). The computational
42 resources are provided by Norwegian Metacenter for Computational Science (NOTUR
43 NN9110k and NN9391k).

44
45
46
47
48
49 **Conflicts of Interest:** The authors declare no conflict of interest.

References

1. L. Wang, M. S. H. Boutilier, P. R. Kidambi, D. Jang, N. G. Hadjiconstantinou and R. Karnik, Fundamental transport mechanisms, fabrication and potential applications of nanoporous atomically thin membranes, *Nat. Nanotechnol.*, 2017, **12**, 509-522.
2. M. Heiranian, A. B. Farimani and N. R. Aluru, Water desalination with a single-layer MoS₂ nanopore, *Nat. Commun.*, 2015, **6**, 8616-8621.
3. R. Devendra and G. Drazer, Gravity driven deterministic lateral displacement for particle separation in microfluidic devices, *Anal Chem*, 2012, **84**, 10621-10627.
4. J. Lee, T. Laoui and R. Karnik, Nanofluidic transport governed by the liquid/vapour interface, *Nat. Nanotechnol.*, 2014, **9**, 317-323.
5. W. Sparreboom, A. van den Berg and J. C. Eijkel, Principles and applications of nanofluidic transport, *Nat. Nanotechnol.*, 2009, **4**, 713-720.
6. B. Liu, C. Wang, J. Zhang, S. Xiao, Z. Zhang, Y. Shen, B. Sun and J. He, Displacement Mechanism of Oil in Shale Inorganic Nanopores by Supercritical Carbon Dioxide from Molecular Dynamics Simulations, *Energy Fuels*, 2017, **31**, 738-746.
7. D. Schaffel, K. Koynov, D. Vollmer, H. J. Butt and C. Schonecker, Local Flow Field and Slip Length of Superhydrophobic Surfaces, *Phys. Rev. Lett.*, 2016, **116**, 134501.
8. M. Ma, F. Grey, L. Shen, M. Urbakh, S. Wu, J. Z. Liu, Y. Liu and Q. Zheng, Water transport inside carbon nanotubes mediated by phonon-induced oscillating friction, *Nat. Nanotechnol.*, 2015, **10**, 692-695.
9. Matthew K. Borg, Duncan A. Lockerby, Konstantinos Ritos and J. M. Reese, Multiscale simulation of water flow through laboratory-scale nanotube membranes, *J. Membrane Sci.*, 2018, **567**, 115-126.
10. D. I. Dimitrov, A. Milchev and K. Binder, Capillary rise in nanotubes coated with polymer brushes, *Ann N Y Acad Sci*, 2009, **1161**, 537-548.
11. T. D. Blake and J. D. Coninck, The influence of pore wettability on the dynamics of imbibition and drainage, *Colloids Surf., A*, 2004, **250**, 395-402.
12. M. Zhang, S. Zhan and Z. Jin, Recovery mechanisms of hydrocarbon mixtures in organic and inorganic nanopores during pressure drawdown and CO₂ injection from molecular perspectives, *Chem. Eng. J.*, 2020, **382**, 122808.
13. P. L. Walls, G. Dequidt and J. C. Bird, Capillary Displacement of Viscous Liquids, *Langmuir*, 2016, **32**, 3186-3190.
14. V. Mirchi, S. Saraji, L. Goual and M. Piri, Dynamic interfacial tension and wettability of shale in the presence of surfactants at reservoir conditions, *Fuel*, 2015, **148**, 127-138.
15. J. Tang, Z. Qu, J. Luo, L. He, P. Wang, P. Zhang, X. Tang, Y. Pei, B. Ding, B. Peng and Y. Huang, Molecular Dynamics Simulations of the Oil-Detachment from the Hydroxylated Silica Surface:

1
2
3 Effects of Surfactants, Electrostatic Interactions, and Water Flows on the Water Molecular Channel
4 Formation, *J. Phys. Chem. B*, 2018, **122**, 1905-1918.

5
6 16. L. Koottungal, 2014 worldwide EOR survey, *Oil Gas J.*, 2014, **112**, 79-91.

7
8 17. X. Zhang, Z. Lu, H. Tan, L. Bao, Y. He, C. Sun and D. Lohse, Formation of surface
9 nanodroplets under controlled flow conditions, *Proc. Nat. Acad. Sci. U.S.A.*, 2015, **112**, 9253-9257.

10
11 18. B. Yuan, W. Wang, R. G. Moghanloo, Y. Su, K. Wang and M. Jiang, Permeability Reduction
12 of Berea Cores Owing to Nanoparticle Adsorption onto the Pore Surface: Mechanistic Modeling and
13 Experimental Work, *Energy Fuels*, 2016, 2017, **31**, 795-804.

14
15 19. H. Zhang, A. Nikolov and D. Wasan, Enhanced Oil Recovery (EOR) Using Nanoparticle
16 Dispersions: Underlying Mechanism and Imbibition Experiments, *Energy Fuels*, 2014, **28**, 3002-3009.

17
18 20. H. Zhang, T. S. Ramakrishnan, A. Nikolov and D. Wasan, Enhanced oil displacement by
19 nanofluid's structural disjoining pressure in model fractured porous media, *J. Colloid Interface Sci.*,
20 2018, **511**, 48-56.

21
22 21. B. Wei, Q. Li, F. Jin, H. Li and C. Wang, The Potential of a Novel Nanofluid in Enhancing Oil
23 Recovery, *Energy Fuels*, 2016, **30**, 2882-2891.

24
25 22. Z. Hu, S. M. Azmi, G. Raza, P. W. J. Glover and D. Wen, Nanoparticle-Assisted Water-
26 Flooding in Berea Sandstones, *Energy Fuels*, 2016, **30**, 2791-2804.

27
28 23. Z. Jin and A. Firoozabadi, Flow of methane in shale nanopores at low and high pressure by
29 molecular dynamics simulations, *J. Chem. Phys.*, 2015, **143**, 104315.

30
31 24. C. Chen, L. Zhuang, X. Li, J. Dong and J. Lu, A many-body dissipative particle dynamics study
32 of forced water-oil displacement in capillary, *Langmuir*, 2012, **28**, 1330-1336.

33
34 25. Q. Xie, M. A. Alibakhshi, S. Jiao, Z. Xu, M. Hempel, J. Kong, H. G. Park and C. Duan, Fast
35 water transport in graphene nanofluidic channels, *Nat. Nanotechnol.*, 2018, **13**, 238-245.

36
37 26. Y. Yang, J. Liu, J. Yao, J. Kou, Z. Li, T. Wu, K. Zhang, L. Zhang and H. Sun, Adsorption
38 behaviors of shale oil in kerogen slit by molecular simulation, *Chem. Eng. J.*, 2020, **387**, 124054.

39
40 27. K. Wu, Z. Chen, J. Li, X. Li, J. Xua and X. Dong, Wettability effect on nanoconfined water
41 flow, *Proc. Nat. Acad. Sci. U.S.A.*, 2017, **114**, 3358-3363.

42
43 28. A. Bera and H. Belhaj, Application of nanotechnology by means of nanoparticles and
44 nanodispersions in oil recovery - A comprehensive review, *J. Nat. Gas. Sci. Eng.*, 2016, **34**, 1284-1309.

45
46 29. J. M. Berlin, J. Yu, W. Lu, E. E. Walsh, L. Zhang, P. Zhang, W. Chen, A. T. Kan, M. S. Wong,
47 M. B. Tomson and J. M. Tour, Engineered nanoparticles for hydrocarbon detection in oil-field rocks,
48 *Energy Environ. Sci.*, 2011, **4**, 505-509.

49
50 30. A. D. N. Darsh T. Wasan, Spreading of nanofluids on solids, *Nature*, 2003, **423**, 156-159.

51
52 31. S. Supple and N. Quirke, Molecular dynamics of transient oil flows in nanopores. II. Density
53 profiles and molecular structure for decane in carbon nanotubes, *J. Chem. Phys.*, 2005, **122**, 104706.

- 1
2
3 32. S. Patel, C. L and B. III, CHARMM Fluctuating Charge Force Field for Proteins: I
4 Parameterization and Application to Bulk Organic Liquid Simulations, *J. Comput. Chem.*, 2003, **25**, 1-
5 15.
6
7
8 33. K. Vanommeslaeghe, E. Hatcher, C. Acharya, S. Kundu, S. Zhong, J. Shim, E. Darian, O.
9 Guvench, P. Lopes, I. Vorobyov and A. D. Mackerell, Jr., CHARMM general force field: A force field
10 for drug-like molecules compatible with the CHARMM all-atom additive biological force fields, *J.*
11 *Comput. Chem.*, 2010, **31**, 671-690.
12
13
14 34. H. J. C. Berendsen, J. R. Grigera and T. P. Straatsma, The missing term in effective pair
15 potentials, *J. Phys. Chem.*, 1987, **91**, 6269-6271.
16
17
18 35. S. Plimpton, Fast Parallel Algorithms for Short-Range Molecular Dynamics, *J. Comput. Phys.*,
19 1995, **117**, 1-19.
20
21 36. X. Wang, S. Xiao, Z. Zhang and J. He, Effect of Nanoparticles on Spontaneous Imbibition of
22 Water into Ultraconfined Reservoir Capillary by Molecular Dynamics Simulation, *Energies*, 2017, **10**,
23 506.
24
25 37. S. Xiao, J. He and Z. Zhang, Nanoscale deicing by molecular dynamics simulation, *Nanoscale*,
26 2016, **8**, 14625-14632.
27
28 38. S. Nosé, A molecular dynamics method for simulations in the canonical ensemble, *Mol. Phys.*,
29 1984, **52**, 255-268.
30
31 39. T. Darden, D. York and L. Pedersen, Particle mesh Ewald: An N·log(N) method for Ewald
32 sums in large systems, *J. Chem. Phys.*, 1993, **98**, 10089-10092.
33
34 40. W. Humphrey, A. Dalke and K. Schulten, VMD: Visual molecular dynamics, *J. Mol. Graph.*,
35 1996, **14**, 33-38.
36
37 41. M. Sedghi, M. Piri and L. Goual, Atomistic Molecular Dynamics Simulations of Crude
38 Oil/Brine Displacement in Calcite Mesopores, *Langmuir*, 2016, **32**, 3375-3384.
39
40 42. B. Ramos-Alvarado, S. Kumar and G. P. Peterson, Hydrodynamic slip in silicon nanochannels,
41 *Phys. Rev. E*, 2016, **93**, 033117.
42
43 43. M. Piri and M. J. Blunt, Three-phase threshold capillary pressures in noncircular capillary tubes
44 with different wettabilities including contact angle hysteresis, *Phys Rev E Stat Nonlin Soft Matter Phys*,
45 2004, **70**, 061603.
46
47 44. C. Chen, K. Lu, X. Li, J. Dong, J. Lu and L. Zhuang, A many-body dissipative particle dynamics
48 study of fluid–fluid spontaneous capillary displacement, *RSC Advances*, 2014, **4**, 6545.
49
50 45. H. Zhang, A. Nikolov and D. Wasan, Dewetting film dynamics inside a capillary using a
51 micellar nanofluid, *Langmuir*, 2014, **30**, 9430-9435.
52
53 46. X. Sun, Y. Zhang, G. Chen and Z. Gai, Application of Nanoparticles in Enhanced Oil Recovery:
54 A Critical Review of Recent Progress, *Energies*, 2017, **10**, 345.
55
56 47. Y. Li, H. Wu and F. Wang, Effect of a Single Nanoparticle on the Contact Line Motion,
57 *Langmuir*, 2016, **32**, 12676-12685.
58
59
60

- 1
2
3 48. Y. Li, F. Wang, H. Liu and H. Wu, Nanoparticle-tuned spreading behavior of nanofluid droplets
4 on the solid substrate, *Microfluidics and Nanofluidics*, 2014, **18**, 111-120.
5
6 49. F. Wang and H. Wu, Enhanced oil droplet detachment from solid surfaces in charged
7 nanoparticle suspensions, *Soft Matter*, 2013, **9**, 7974-7980.
8
9 50. J. C. Melrose and C. F. Brandner, Role of Capillary Forces in Determining Microscopic
10 Displacement Efficiency for Oil Recovery by Waterflooding, *J. Can. Petrol.*, 1974, **4**, 54-62.
11
12 51. X. Wang, Z. Zhang, O. Torsaeter and J. He, Atomistic insights into the nanofluid transport
13 through an ultra-confined capillary, *Phys. Chem. Chem. Phys.*, 2018, **20**, 4831-4839.
14
15 52. X. Wang, S. Xiao, Z. Zhang and J. He, Transportation of Janus nanoparticles in confined
16 nanochannels: a molecular dynamics simulation, *Environ. Sci.: Nano*, 2019, **6**, 2810-2819.
17
18 53. X. Wang, S. Xiao, Z. Zhang and J. He, Displacement of nanofluids in silica nanopores:
19 influenced by wettability of nanoparticles and oil components, *Environ. Sci.: Nano*, 2018, **5**, 2641-2650.
20
21
22
23
24
25
26
27
28
29
30
31
32
33
34
35
36
37
38
39
40
41
42
43
44
45
46
47
48
49
50
51
52
53
54
55
56
57
58
59
60

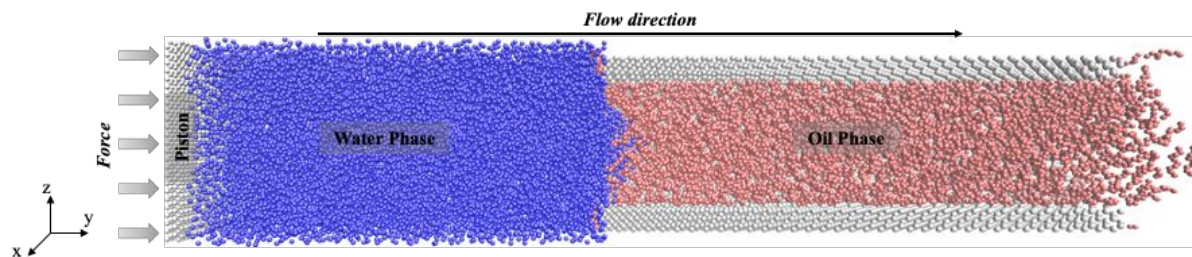


Figure 1 Representative atomistic model of a two-phase displacement system. The colors of atoms represent oil (pink), water (blue), silicon (light grey) and piston (light grey), and apply to the following snapshots.

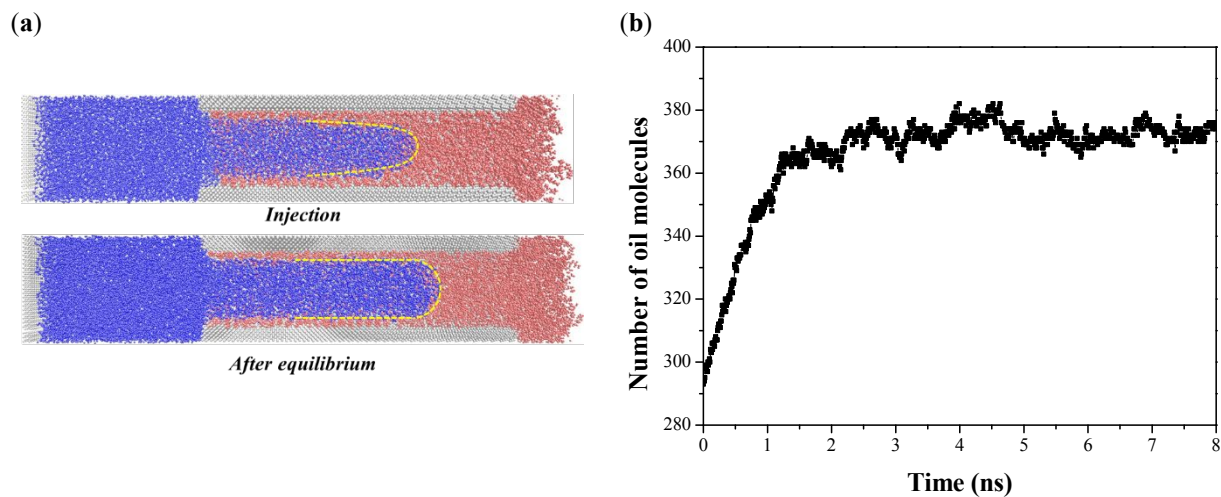


Figure 2 (a) Flow snapshots for injection at 4.0 ns and equilibrium system after 4.0 ns with fixed piston.

(b) The number of oil molecules displaced out of the capillary as a function of time at equilibrium.

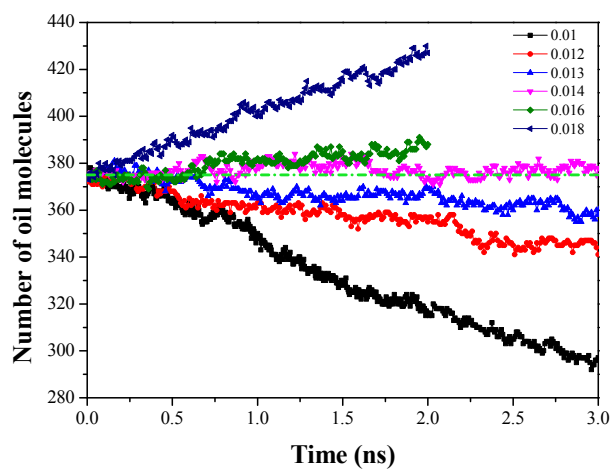


Figure 3 The number of oil molecules displaced out of the capillary with the pumping pressure exerting on piston decreased from 0.018 to 0.01 kcal/mol/Å.

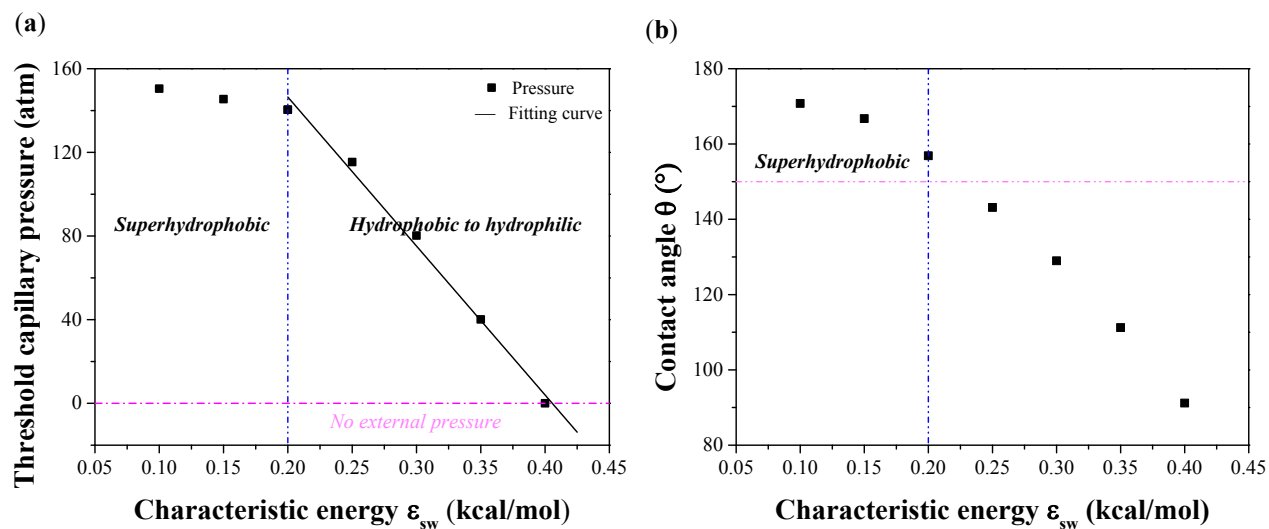


Figure 4 (a) Threshold capillary pressure and (b) three phase contact angle as a function of characteristic energy ϵ_{sw} between water and capillary.

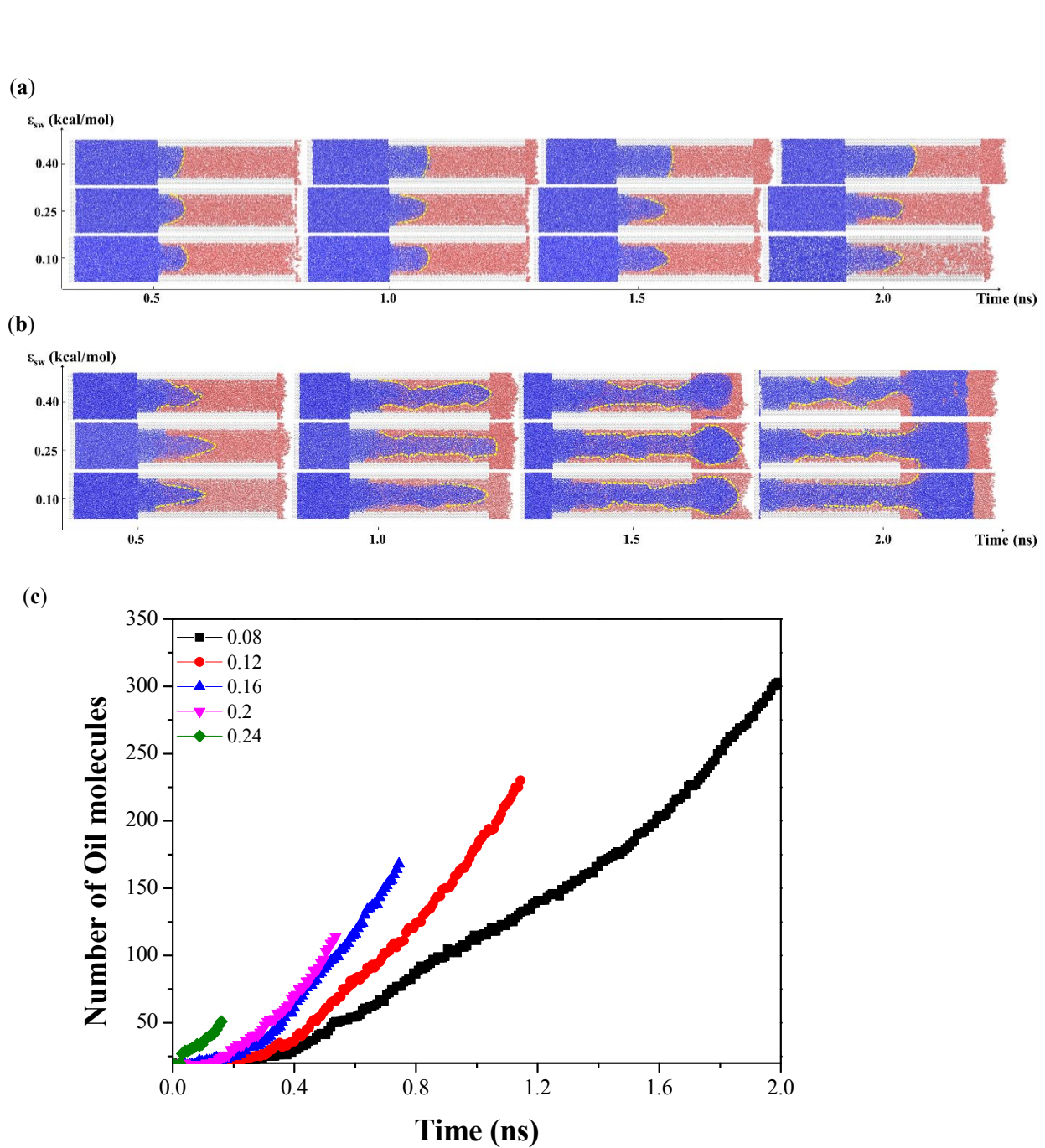


Figure 5 Flow snapshots of forced water-oil displacement in capillary with varied characteristic energy ε_{sw} : (a) at low pumping pressure ($f=0.02$ kcal/mol/Å); (b) at high pumping pressure ($f=0.20$ kcal/mol/Å). The meaning of colors is same as in Figure 2, while the yellow curve shows fluids interface. (c) Oil molecules outside the capillary with different pumping pressure, $\varepsilon_{sw}=0.1$ kcal/mol.

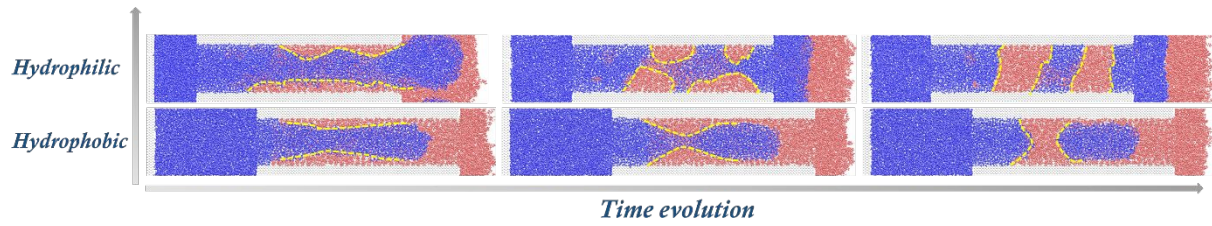


Figure 6 Dynamic flow configurations after water flooding in hydrophilic and hydrophobic capillary.

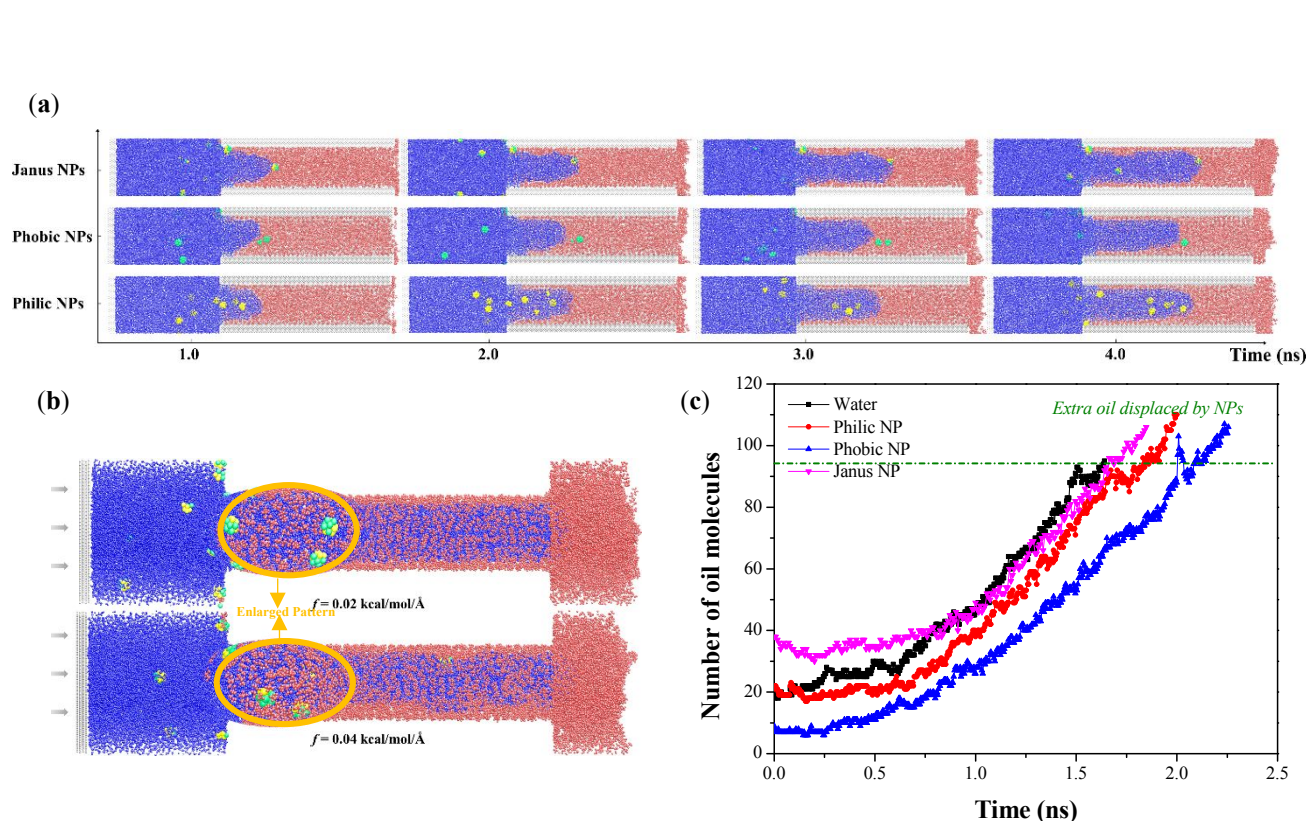


Figure 7 The effect of NPs on the displacement process in capillary $\varepsilon_{sw} = 0.25$ kcal/mol. (a) Snapshots of forced nanofluids displacement with different kinds of NPs in hydrophobic capillary, (b) snapshots for fluids with Janus NPs at different external force on piston; and (c) the number of oil molecules outside capillary with and without NPs, and the bulge of the capillary in orange circle is intended to enlarge the Janus nanoparticles to display them in the capillary. The meaning of colors for NPs: hydrophilic NPs (yellow), hydrophobic (green), and Janus NP (hydrophilic part is yellow and hydrophobic part is green).

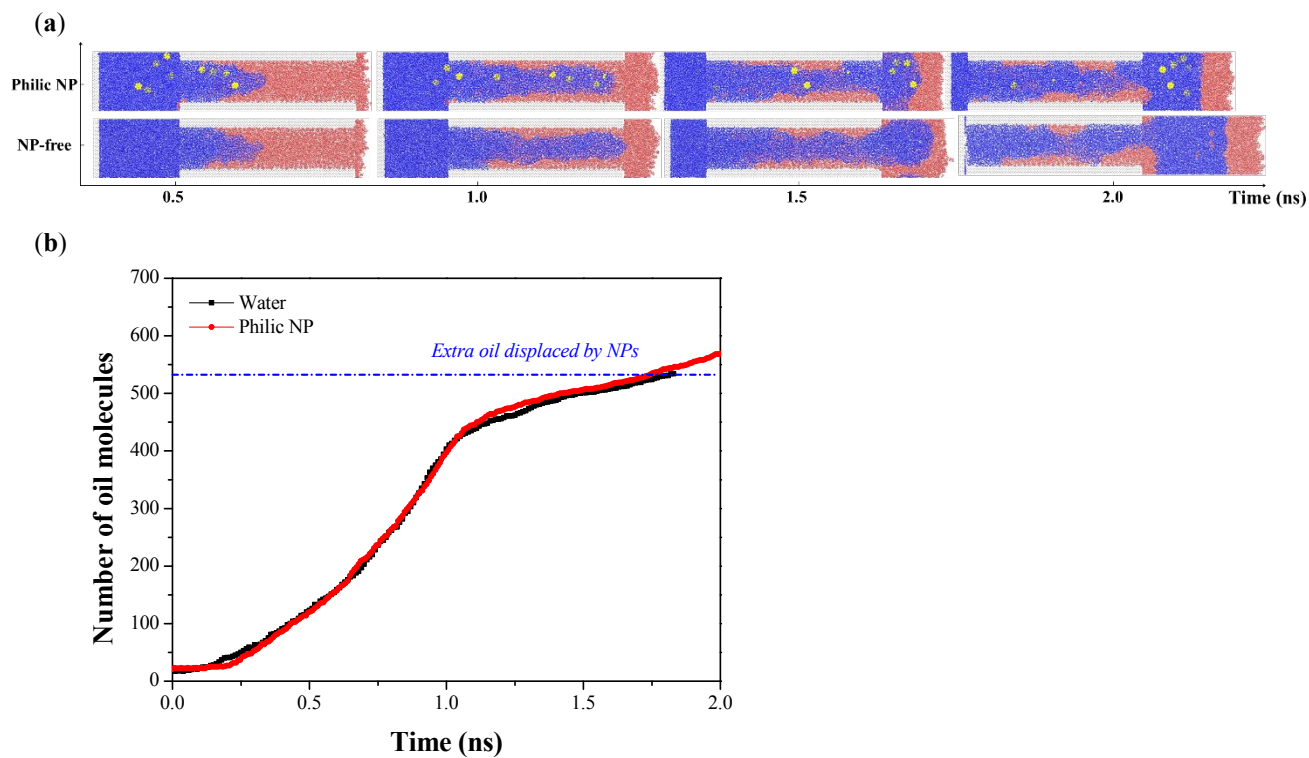
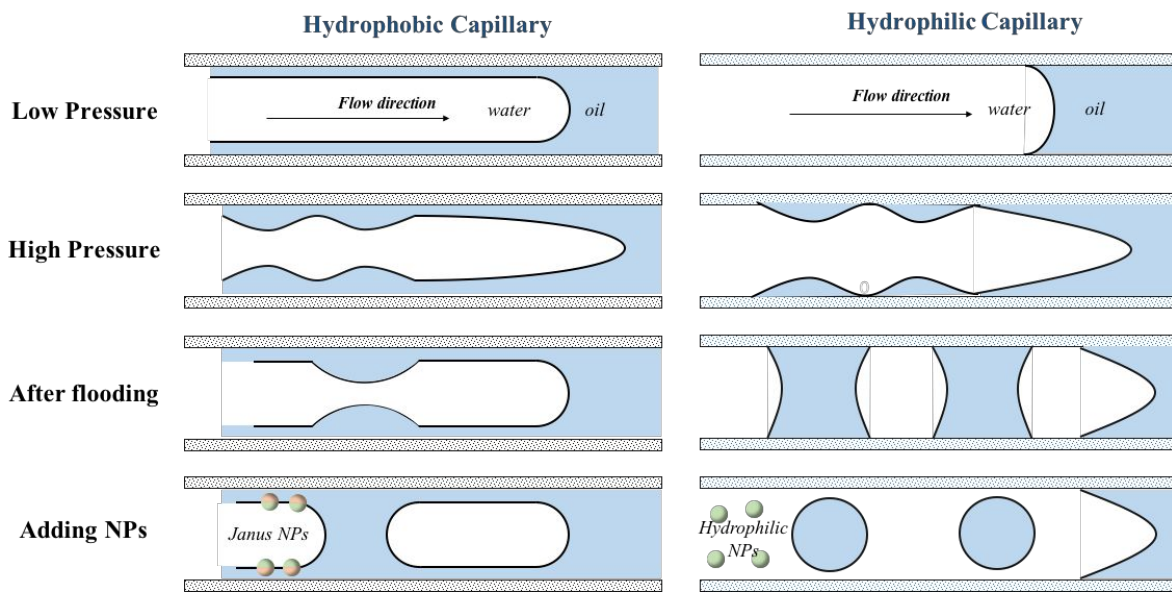


Figure 8 (a) Snapshots of forced nanofluids displacement with and without hydrophilic NPs in hydrophilic capillary; and (b) the content of oil molecules outside capillary with and without NPs, $\epsilon_{sw} = 0.4$ kcal/mol when the piston moves to the entrance of the capillary.

Graphic



Supporting information

Insight into the Pressure-induced Displacement Mechanism for Selecting Efficient Nanofluids in Various Capillaries

Xiao Wang ¹, Zhiliang Zhang ¹, Jun Zhang ² and Jianying He ^{1,*}

¹ NTNU Nanomechanical Lab, Department of Structural Engineering, Faculty of Engineering, Norwegian University of Science and Technology (NTNU), 7491 Trondheim, Norway

² School of Materials Science and Engineering, China University of Petroleum, Qingdao, Shandong, 266580 China

* Correspondence: jianying.he@ntnu.no ; Tel.: +47-93804711

S1. Adsorption Behavior of Decane

The orientation of decane is important to understand the displacement process. Here, the orientation of decane molecules at capillary wall and water-oil interface are analyzed separately. For decane adsorption on capillary wall, the equilibrium configuration is captured from the trajectory of molecular dynamics simulations. As shown in Figure S1, the decane molecules exhibit an obvious layer by layer adsorption on capillary. This phenomenon is consistent with our previous works and other simulation studies ^{1,2}.

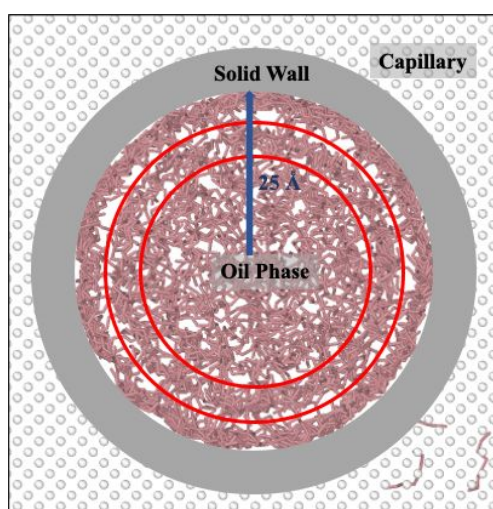


Figure S1 The adsorption configuration of oil phase in capillary. The gray color represents the solid wall of the capillary. The red lines depict the adsorption layers of decane molecules in the capillary.

Meanwhile, the orientation of decane with respect to the dynamical oil/water interface is analyzed qualitatively by the equilibrium configurations. The hydrophobic capillary is taken as an example. As shown in Figure S2(a) and (b), the oil/water interface in hydrophobic capillary can be divided into two parts, i.e., the interfaces near (cyan, Part I) and away from (yellow, Part II) the capillary. For Part I, during the flooding process, decane always adsorbs parallel to the solid surface due to its strong interaction with hydrophobic wall (Figure S2(b)). However, for part II, different orientations are observed (Figure S2(c)), i.e., normal to interface (blue), parallel to interface (yellow), and tilted to the interface (green). Moreover, along with the simulation time, decane molecules involve large diffusions, and their orientations change randomly.

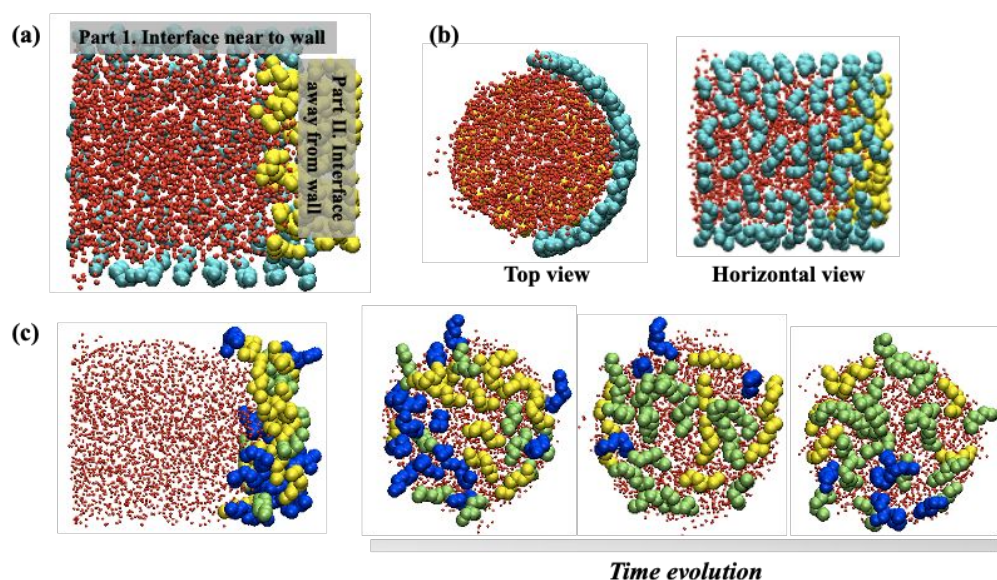


Figure S2 Configurations of water-oil interface in the nanochannel. (a) water-oil interface; (b) top view and horizontal view; (c) Part II from horizontal view and top views; The colors in (a) and (b): water (red); oil in part I (cyan); oil in part II (yellow); The colors in (c); water (red); oil normal to interface (blue), oil parallel to interface (yellow) and oil tilted to interface (green).

S2. Verification of Model

The fluids properties in the system are verified by viscosity of water and interfacial tension of decane/water. This process is also described in our previous simulations.

The viscosity of water can be derived by Einstein relation ^{2,3}.

$$\eta = \frac{k_B T}{3\pi r_w D} \quad (S1)$$

where k_B is the Boltzmann constant, T is simulation temperature, r_w is the molecular diameter, and D is diffusion coefficient of fluid. According to previous simulation, self-diffusion coefficient for water is $2.67 \times 10^{-9} \text{m}^2 \text{s}^{-1}$, which matches well with experimental data (2.09 - $2.66 \times 10^{-9} \text{m}^2 \text{s}^{-1}$) and other simulation results ⁴. The calculated viscosity of water is $0.9622 \text{MPa} \cdot \text{s}$ under 298.15K using Eq.S1, in good agreement with experimental value of $1.0 \text{MPa} \cdot \text{s}$. The other important property is water-oil interfacial tension. The interfacial tension of water-oil is derived by subtracting mean tangential stress tensors (i.e., P_{xx} and P_{yy}) from the normal one (i.e., P_{zz}) ⁵.

$$\sigma_{wo} = \frac{1}{2} L_z \left\langle P_{zz} - \frac{1}{2} (P_{xx} + P_{yy}) \right\rangle \quad (\text{S2})$$

where L_z is the length of simulation box in z axis. The calculated interfacial tension for decane/water interface is $50.54 \pm 1.28 \text{mN/m}$, in good agreement with the experimental value of 51.98mN/m ⁶.

S3. Three-phase Contact angle

To calculate three-phase contact angle to assess the wettability of capillary, the water and oil were initially placed into the capillary, and the piston was fixed. Here, the characteristic energy ϵ_{sw} was tuned from 0.1 to 0.4kcal/mol , forming hydrophobic to hydrophilic capillary, and other parameters were kept the same as those in Section 2. The detailed configuration is shown in Figure S3. The 4.0ns simulation time was adopted to equilibrium the system, and the last 2.0ns was analyzed to calculate three-phase contact angle.

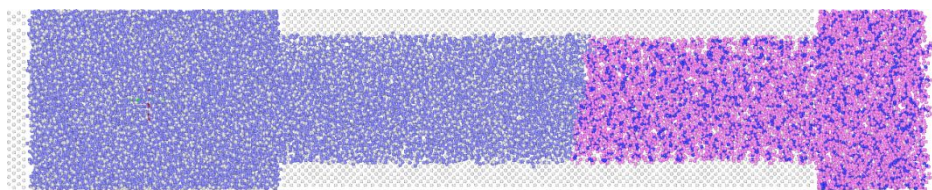


Figure S3 Simulation model to calculate three-phase contact angle in different capillary. The colors in Figure: piston and capillary (white); water (blue); oil (purple and blue).

According to our previous study, ⁷ contact angle will have large fluctuation and reach a dynamic equilibrium value during displacement. To determine the contact angle, liquid in capillary is firstly divided into cylindrical shells, and then is subdivided by certain thickness 1.5Å . The number of shells should be constrained to ensure that each shell contains enough water molecules to give a uniform density. The density of water in each shell as a function of the distance l into the pore is analyzed. The advancing end of each shell is located at where the

density is below a cutoff value of half the water density. The contact angle is then obtained from the tangent to a circular fit to the profile.⁷ Here, the three-phase contact angle in capillary with $\varepsilon_{sw} = 0.1$ kcal/mol is shown in Figure S4. From Figure S4, it can be seen that contact angle for fluids in the capillary is almost stable, and the relative equilibrium value can be obtained. The same method can be applied to other capillary and the results are in the Figure 4(b) in the main text.

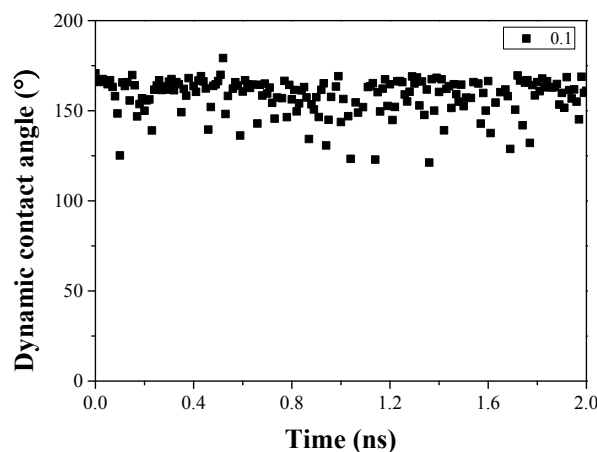


Figure S4 Dynamic three-phase contact angle for fluids in capillary with $\varepsilon_{sw} = 0.1$ kcal/mol.

S4. Relationship between position of piston and threshold capillary pressure

Figure S5 is a schematic diagram about two-phase displacement process in the nanochannel. During the fluid flow process, there will be viscous force, capillary force and external force in this system. During the fluid flow process, the force balance can be described as Eq.S3⁸.

$$P_{applied} = \frac{2\gamma_{AB}\cos\theta}{R} - \frac{8\eta_A}{R^2}l_A\frac{dl_A}{dt} - \frac{8\eta_B}{R^2}l_B\left(-\frac{dl_B}{dt}\right) \quad (S3)$$

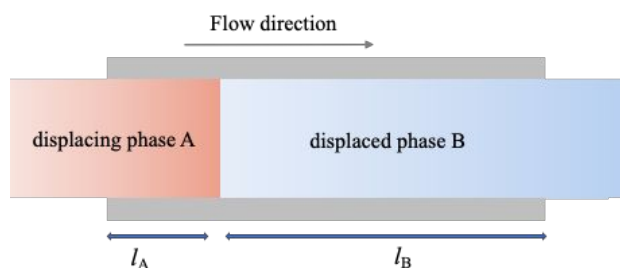


Figure S5 The schematic for two-phase displacement process in nanochannel

where $P_{applied}$ is applied force, γ_{AB} is interfacial tension between A and B, θ is three-phase contact angle, R is capillary radius, η_A and η_B are viscosity of phase A and B, respectively. l_A and l_B are length of phase A and B in capillary, and t is simulation time.

Considering no velocity for displacing phase A and B at the equilibrium state, then the equation can be simplified to

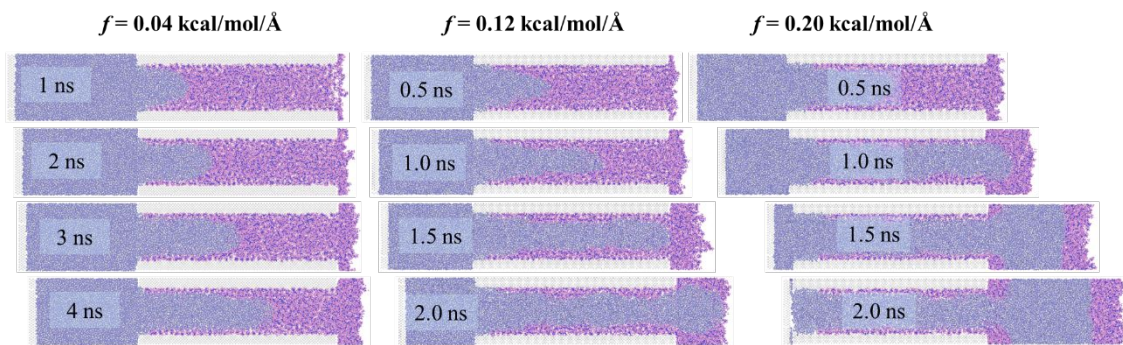
$$P_{threshold} = \frac{2\gamma_{AB}\cos\theta}{R} \quad (S4)$$

From Eq.S4, it can be seen that the threshold capillary pressure only relates to the interfacial tension γ_{AB} , contact angle θ , and capillary radius R , which it is not affected by the position of the piston.

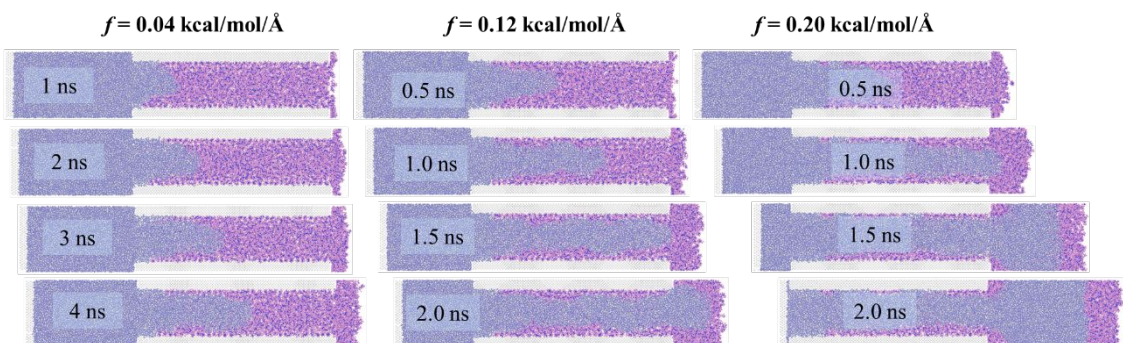
S5. Influence of pumping pressure on forced displacement process in capillary

For the influence of pumping pressure on the forced displacement process, the configurations of forced water-oil displacement in varied capillary under different pumping pressure are shown in Figure S6.

$\epsilon_{sw} = 0.15$ kcal/mol



$\epsilon_{sw} = 0.30$ kcal/mol



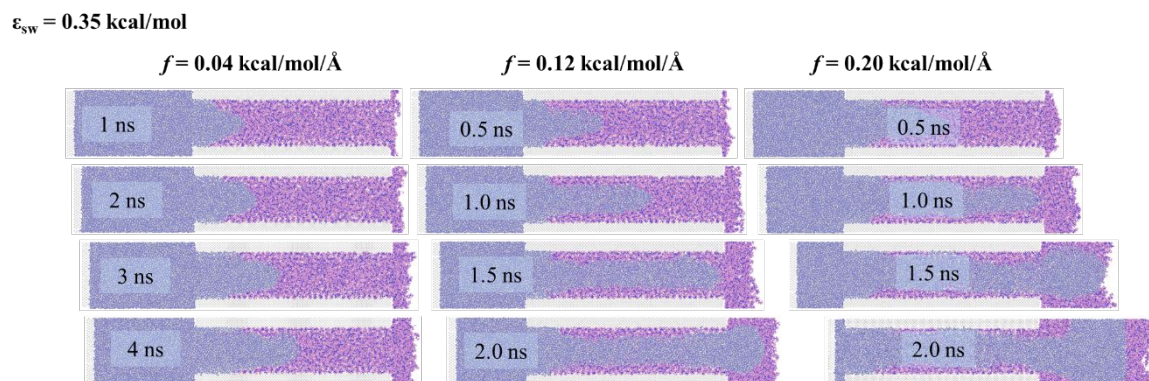


Figure S6 Flow snapshots for forced water-oil displacement in different kinds of capillary under different pumping pressure. The colors are the same as in Figure S3.

S6. Simulation details of forced displacement by nanofluids

To study the influence of nanoparticles on the forced displacement process, 16 spherical NPs with a diameter of 7.0 \AA were well distributed in water phase. The main characteristic energies for NPs are interactions with water ϵ_{nw} and NP-NP ϵ_{nn} . The characteristic energy for NP-NP ϵ_{nn} was set relatively small as 0.01 kcal/mol for a weak interaction between NPs. And ϵ_{ns} was chosen 0.7 kcal/mol designating the strong interaction between solid capillary and NPs. By tuning characteristic energy ϵ_{nw} between NPs and water, hydrophobic, Janus, and hydrophilic NPs were obtained, listed in Table S1. Then other parameters were kept the same as in the main text^{2,9}.

Table S1 Force fields parameters for NPs with water ϵ_{nw} , oil ϵ_{no} , and capillary ϵ_{ns} .

Characteristic energy, kcal/mol	Water	Oil	Capillary
Hydrophilic NPs	0.6	0.05	0.7
Janus NPs (hydrophobic)	0.01	0.2	
Janus NPs (hydrophilic)	0.4	0.01	
Hydrophobic NPs	0.05	0.6	

S7. Displacement mechanism of nanoparticles in capillary

Via analyses of displacement length, motion behavior and capillary pressure etc. in our previous simulations^{2,9}, displacement mechanisms of different NPs during displacing process are summarized in Figure S7. In Figure S7, the first line is the type of NPs. The second line

shows the motion behavior for NPs in capillary, i.e., dispersed in water, adsorbed onto capillary, aggregated bigger micelles, or self-assembled at fluids interface. The last line gives the dominating displacement mechanism for NPs displaced in capillary.

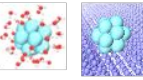
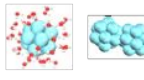
Type of NPs	 hydrophobic	 mix	 hydrophilic	 Janus
Behavior				
Mechanism	Viscosity Capillary	Viscosity	Viscosity	Capillary

Figure S7 Summarized of the motion behavior and displacement mechanism of different NPs in capillary.

References

1. H. Yan and S. Yuan, Molecular Dynamics Simulation of the Oil Detachment Process within Silica Nanopores, *J. Phys. Chem. C.*, 2016, **120**, 2667-2674.
2. X. Wang, Z. Zhang, O. Torsaeter and J. He, Atomistic insights into the nanofluid transport through an ultra-confined capillary, *Phys. Chem. Chem. Phys.*, 2018, **20**, 4831-4839.
3. J. A. Thomas and A. J. H. McGaughey, Reassessing Fast Water Transport Through Carbon Nanotubes, *Nano Lett*, 2008, **8**, 2788-2793.
4. Y. Yan, X. Wang, Y. Zhang, P. Wang, X. Cao and J. Zhang, Molecular dynamics simulation of corrosive species diffusion in imidazoline inhibitor films with different alkyl chain length, *Corros. Sci.*, 2013, **73**, 123-129.
5. Y. Zhang, S. E. Feller, B. R. Brooks and R. W. Pastor, Computer simulation of liquid/liquid interfaces. I. Theory and application to octane/water, *J. Chem. Phys.*, 1995, **103**, 10252-10266.
6. F. Leroy, Revisiting the droplet simulation approach to derive force-field parameters for water on molybdenum disulfide from wetting angle measurements, *J. Chem. Phys.*, 2016, **145**, 164705-164716.
7. X. Wang, S. Xiao, Z. Zhang and J. He, Effect of Nanoparticles on Spontaneous Imbibition of Water into Ultraconfined Reservoir Capillary by Molecular Dynamics Simulation, *Energies*, 2017, **10**, 506.
8. C. Chen, K. Lu, X. Li, J. Dong, J. Lu and L. Zhuang, A many-body dissipative particle dynamics study of fluid–fluid spontaneous capillary displacement, *RSC Advances*, 2014, **4**, 6545-6555.
9. X. Wang, S. Xiao, Z. Zhang and J. He, Transportation of Janus nanoparticles in confined nanochannels: a molecular dynamics simulation, *Environ. Sci.: Nano*, 2019, **6**, 2810-2819.

Graphics

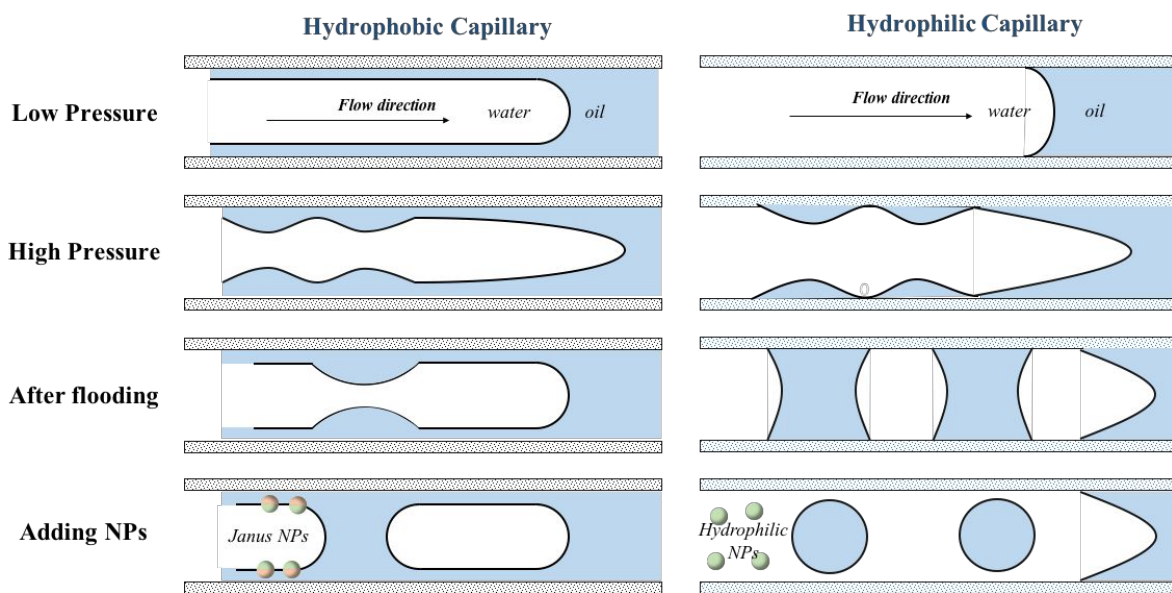


Table of contents: Pressure-induced displacement mechanism in hydrophobic and hydrophilic capillary

1
2
3
4
5
6
7
8
9
10
11
12
13
14
15
16
17
18
19
20
21
22
23
24
25
26
27
28
29
30
31
32
33
34
35
36
37
38
39
40
41
42
43
44
45
46
47
48
49
50
51
52
53
54
55
56
57
58
59
60